JOURNAL OF PROPULSION AND POWER
Vol. 16, No. 5, September–October 2000

Effect of Inlet Turbulence and Premixer Length on Fuel Distribution in Swirling Gas-Turbine Premixer

S. F. Frey,* A. R. Eaton,* D. M. Cusano,* M. W. Plesniak,† and P. E. Sojka‡
Purdue University, West Lafayette, Indiana 47907-1003

The mixing characteristics of a production gas-turbine combustor premixer have been investigated using a planar Mie-scattering imaging technique. Specifically, the effects of introducing controlled inlet grid turbulence (intensity and scale) and varying premixer length on large-scale mixing were independently studied. Baseline data acquired for a particular swirler configuration indicated a strong fuel concentration gradient in the annulus, with a maximum at the centerbody and decreasing outward. The measured fuel concentration, or equivalence ratio, also varied circumferentially, by as much as 45% over the entire premixer exit plane. The circumferential fuel concentration profiles showed that improved mixing with increased turbulence intensity was realized for most angular locations. Premixer length extensions of 2.5 and 5.0 cm, corresponding to 0.53 and 1.06 hydraulic diameters, respectively, resulted in a considerable improvement in mixing, accompanied by significant structural changes in the scalar field. The circumferential variations were reduced up to 30% for the 5.0-cm extension case. Radial fuel concentration gradients were also reduced by 50%. Overall, increased residence time was a significantly more effective means of mixing enhancement than introducing moderate levels of freestream turbulence.

Nomenclature

b = turbulence grid bar diameter, mm
D_h = hydraulic diameter, m
L = premixer length, m
Lx = integral length scale, m
M = turbulence grid mesh size, cm
N = number of revolutions, dimensionless
r = radial position, m
S = circumferential distance, m
SN = swirl number, dimensionless
SR = turbulence grid solidity ratio, dimensionless
s = unmixedness parameter, dimensionless
Tu = turbulence intensity, %
t = time, s
U_s = local mean axial velocity, m/s
u' = rms value of fluctuating axial velocity, m/s
V_a = air velocity, m/s
W_s = local mean tangential velocity, m/s
x = axial distance downstream of grid, m
θ = swirl vane angle or angle of wedge revolution, deg
ϕ = input equivalence ratio, dimensionless

I. Introduction

INCREASINGLY stringent regulations are requiring gas-turbine manufacturers to reduce NO_X emissions. A spectrum of NO_X limits for industrial gas turbines exists, including 150, 75, 65, 42, 25, and 9 ppm depending on the fuel used, the location of the facility, the type of facility, and whether a state air permit is required.[1] The ultra-low NO_X levels were consistently met only with high capital cost methods of selective catalytic reduction (SCR) and water injection.[2] However, dry NO_X control through lean-premixed combustion promises to be a more economical means of achieving ultra-low NO_X (Ref. 3).

A popular method for reducing NO_X is to control the temperature of the flame zone, usually through lean combustion. Early designs employing lean combustion produced promising results, but did not approach NO_X levels predicted by computational simulations.

A substantial portion of the discrepancy between test data and model predictions was attributed to the presence of combustion-zone hot spots that resulted from incomplete mixing of the fuel and air in localized regions.[3] It has, therefore, become clear that improved mixing is essential for reducing combustor emissions to levels that comply with mandated air quality standards. Parametric studies must be performed to understand how design features influence mixing characteristics. One parameter to be investigated is residence time. Turbulence intensity and scale are also expected to have an effect on mixing processes.

Fundamental studies of turbulent boundary layers have revealed significant effects of elevated freestream turbulence on skin friction and heat transfer. These effects depend not only on the turbulence intensity but also upon the length scales of the turbulence. Correlations developed by Hancock and Bradshaw[4] and Blair[5] include the turbulence intensity and energy length scale, whereas that proposed by Ames and Moffat[6] includes the turbulence intensity and turbulence dissipation length scale. Elevated freestream turbulence is also known to have a significant effect in gas-turbine applications, most notably on turbine blade surface heat transfer. (Levels of turbulence exiting a gas-turbine combustor of up to 20% are not uncommon, see Refs. 7–9.) The correlation of Ames and Moffat[6] was applied by Thole and Bogard[10] to many different data sets and found to perform well in gas-turbine film cooling applications. Several cascade tests and other film-cooling-oriented studies with elevated freestream turbulence have been reported, including Refs. 11–15. All show that turbulence intensity and length scale are important.

Free-shear layers are also sensitive to turbulence length scale and intensity. For example, the study of bluff body wakes by Wolochuk et al.[16] illustrated the importance of both integral length scale and intensity. Some of the same mechanisms responsible for modifications to the film-cooling characteristics and bluff-body wakes are also expected to play a role in modifying the mixing of air and fuel in the swirling premixer in the current study.

The goals of the current experimental investigation were twofold: first, establish a baseline by investigating the level of mixedness for a representative gas turbine-swirler-mixer, and second, evaluate the effect of premixer length (residence time), along with inlet turbulence intensity and scale on fuel-air mixing. (Premixer length cannot be increased arbitrarily without eventually experiencing

Received 25 January 1999; revision received 20 July 1999; accepted for publication 3 September 1999.

*Graduate Research Assistant, Maurice J. Zucrow Laboratories, School of Mechanical Engineering.
†Associate Professor, Maurice J. Zucrow Laboratories, School of Mechanical Engineering, Senior Member AIAA.
‡Professor, Maurice J. Zucrow Laboratories, School of Mechanical Engineering; sojka@ecn.purdue.edu.

detrimental effects of combustion instability and noise.) These goals are accomplished by using a laser-based technique to measure mixedness under simulated engine conditions in typical production hardware.

II. Experimental Apparatus

The mixing performance of a multivaned axial premixer-swirler was evaluated. The swirler, shown schematically in Fig. 1a, is of the type commonly used in industrial gas-turbine engines. It has an axisymmetric annular airflow passage, into which extend a number of radially oriented fuel spray tubes. Each spray tube has two sets of fuel delivery orifices drilled into it; one set is parallel to the premixer axis, and the other is perpendicular, as shown in Fig. 1b. The premixer is 8.89 cm long, with an outer diameter of 6.35 cm and a centerbody 4.0 cm in diameter. This gives an annulus of 2.35 cm and a hydraulic diameter D_h of 4.70 cm. The premixer swirl vanes are set at an angle of 48 deg, resulting in a swirl number value of 1.1 (swirl number is defined as $SN = U_s / W_s = \tan\theta$). The swirler was operated at conditions typical of those found in an actual gas-turbine engine. See Table 1 for details.

Inlet turbulence effects were assessed by imposing controlled, grid-generated turbulence on the airstream that flowed into the premixer. Controlled turbulence was generated by placing biplanar grids of circular section bars upstream of the premixer (see Fig. 2a.) A polyvinyl-chloride(PVC) mount was attached to the premixer inlet, with grid position inside the mount adjusted by acrylic spacers.

Two grids were used, each with a different mesh size, to produce different integral length scales (approximated as the mesh size of the grid[17]). Grid geometrical characteristics are presented in Table 2.

Turbulence intensities of approximately 2.5, 4, and 8% were obtained for the $M = 0.41$-cm grid at downstream locations of 1.2, 3.8, and 10 cm, respectively. (These locations correspond to x/M values of 2.9, 9.3, and 24.) Turbulence intensities of approximately 2 and 4% were obtained at axial positions of 0.63 and 3.8 cm for the $M = 0.16$-cm grid. (These positions correspond to x/M values of 3.9 and 24.)

The turbulence intensity was defined as u'/U_s. Rough estimates of turbulence intensity could be made using correlations for the decay of grid turbulence,[17] hot-wire anemometry measurements were required to determine the actual values. It was necessary to measure the turbulence intensity decay with streamwise distance because the aforementioned relations for the decay of grid turbulence are strictly valid only far enough downstream of the grid, i.e., $20 > x/M > 150$.

The influence of premixer length was investigated by adding two different extensions to the premixer body. The premixer centerbody and outer casing were first extended by 2.5 cm, and then by 5.0 cm (see Fig. 2b.) The extensions effectively add length, while maintaining the same sudden dump flow geometric configuration.

The mixing evaluation facility is unique in that it allows experiments to be performed for swirlers having practical fuel and airflow rates. Total mass-flow rate values considered here ranged up to 150 g/s (0.33 lbm/s).

Table 1 Experimental operating conditions

Property	Air	Simulated fuel
Temperature, K	295	295
Density, kg/m^3	1.23	1.07
Pressure, kPa	100	100
Mass-flow rate, kg/s	0.143	0.025
Velocity, m/s	61	152
Mach number	0.17	0.33
Mass-flow rate ratio	0.037	0.037
Momentum ratio	0.110	0.110

Table 2 Turbulence grid characteristics

Grid number	M, cm	b, mm	SR
1	0.41	0.89	0.39
2	0.16	0.23	0.27

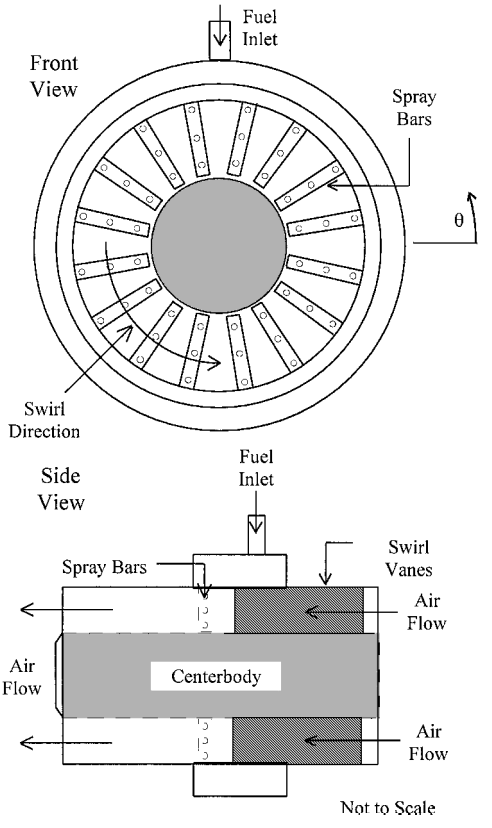

Fig. 1a Swirler schematic.[18]

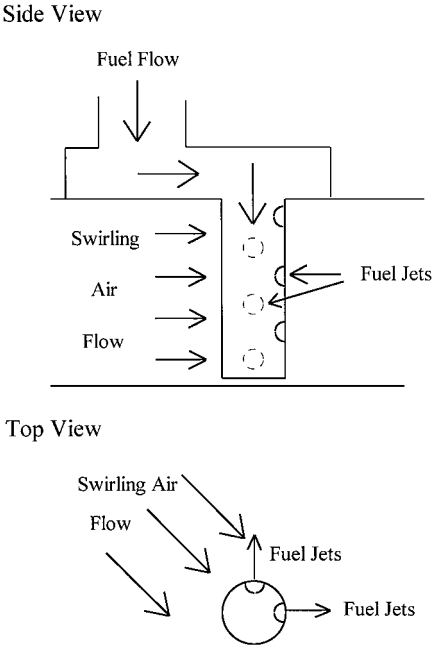

Fig. 1b Schematic of fuel jets in the swirling airflow.[19]

Air and simulated fuel are supplied to the swirler from a compressed air source. In these cold flow experiments the fuel is simulated using air marked with tracer particles. The air supply system consists of inlet compressed air from the source, an isolation valve, a regulator, a pilot valve with pressure taps, an orifice plate with pressure and temperature taps, a filter, a flow control valve, a plenum, and dial pressure gauges. Details of this system are provided by Frey[18] and Eaton.[19]

The airflow rate is measured using an orifice plate that was designed per American Society of Mechanical Engineers (ASME) specifications.[20] A pressure transducer is used to measure the

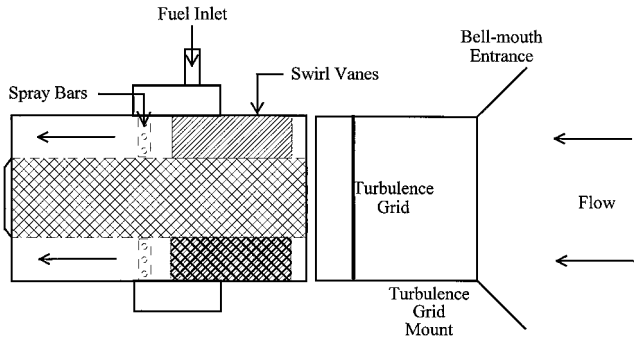

Fig. 2a Inlet turbulence grid position relative to premixer.

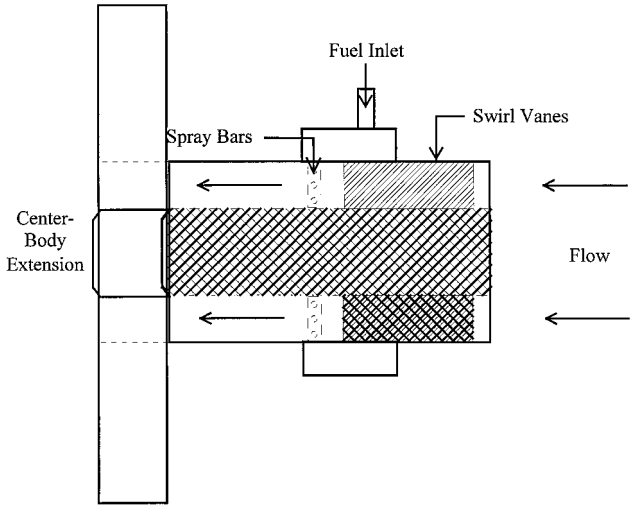

Fig. 2b Premixer length extension hardware.

pressure drop across the plate (flange taps, conforming to ASME specifications), whereas a type-T thermocouple measures temperature. The flow is filtered downstream of the orifice plate by a Parker–Hannifin model FSF6-3-2-F air filter to remove any oil droplets or particles larger than 0.3 μm; it then passes through a plenum. The cross-sectional area of the plenum is approximately 35 times that of the pipe and is approximately 18 pipe diameters in length. The test article is mounted to the end of the plenum.

The fuel supply system is comprised of inlet compressed air, a solenoid valve, an orifice plate, a filter, and a flow control valve. The flow rate is measured using an orifice plate designed per ASME specifications and controlled using a ball valve. A pressure transducer measures the pressure drop across the orifice plate. Flange taps (located according to ASME specifications) were employed, and a type-T thermocouple was used to measure the temperature.

A reverse cyclone seeder design based on the work of Kounalakis[21] was used to seed the fuel stream (air) with tracer particles. The Al_2O_3 tracer particles had a mean diameter of 1 μm. The size distribution is reported by Frey[18] and Eaton.[19] Extinction measurements were performed to optimize seeder performance and to evaluate the seed particle concentration fluctuations (unsteadiness).[19]

The imaging apparatus used to obtain mixing data consists of four subsystems: 1) a Lumonics HLS-0.6 (30-ns duration, 0.6 J/pulse) ruby laser, 2) laser-sheet forming/positioning optics, 3) two Panasonic model GP-MF-552 CCD cameras (480 × 640 pixel × 256 gray scale), and 4) two Gateway 486 personal computers (PC) with data translation DT2867-LC frame grabber boards. These systems are summarized by Eaton et al.[22] and discussed in detail in Frey[18] and Eaton.[19]

An optical system is used to form a laser sheet and to position it in the exit plane of the mixer normal to the main flow direction. The vertical location of the beam is then adjusted such that its centerline intersects the swirler centerline. Two charged-coupled device (CCD) cameras were used to image the laser sheet digitally. One camera positioned downstream and normal to the laser sheet was focused on it and captured the mixing image created by laser light scattering from the aluminum oxide particles used to seed the fuel stream. The other camera was used to acquire the laser-sheet profile prior to entering the test cell to correct for intensity variations in the sheet. The principles of operation and benchmarking of the mixing system are provided by Eaton et al.[22]

Two image-processing boards were used to acquire the images captured by the CCD cameras simultaneously. Each board was installed in a separate PC. They were triggered simultaneously by the output of the laser. The image-processing software consists of commercial frame grabbing software (Data Translation's Global Lab Image) and image-processing FORTRAN code written specifically for this study. Details are provided by Eaton et al.,[22] Frey,[18] and Eaton.[19]

Several sources of uncertainty must be considered when analyzing the data presented here. They include seeder concentration fluctuations, fuel and airflow rate fluctuations, pixel response nonlinearity and nonuniformity, the laser correction curve fit, pulse energy variations, and the centerbody halo effect.[18,19]

Seeder concentration fluctuations were approximately 10% of the mean. Fuel and airflow rates fluctuated by approximately 3% over any given data set of 25 images (about 10 min of run time). Camera pixel response tests[18,19] showed an uncertainty in linearity and uniformity of 5% over the entire dynamic range of the camera. A cubic-spline fit of the laser profile data was performed when processing the data and determining the pulse energy. The average difference between the fit and the actual data was 2%. The pulse energy was determined from the same data and had an uncertainty of 5%. Finally, a halo effect, caused by laser light scattered by the premixer centerbody, introduced an offset in the absolute pixel intensity of 6 to 12%. However, this shift was consistent in all of the images acquired in a run and represents a dc shift in the pixel values. The root-sum square[23] of all of the uncertainties mentioned was calculated to determine the total uncertainty Un:

$$Un = \sqrt{\left(\frac{\delta C'}{C'}\right)^2 + \left(\frac{\delta V_{\text{air}}}{V_{\text{air}}}\right)^2 + \left(\frac{\delta V_{\text{fuel}}}{V_{\text{fuel}}}\right)^2 + \left(\frac{\delta P_R}{P_R}\right)^2 + \left(\frac{\delta E_{\text{fit}}}{E_{\text{fit}}}\right)^2 + \left(\frac{\delta E}{E}\right)^2 + \left(\frac{\delta \phi_{\text{rel}}}{\phi_{\text{rel}}}\right)^2} \tag{1}$$

The resulting value for the mixing data presented here is $Un = \pm 19\%$.

Because the CCD pixel intensity is directly proportional to the number of particles in the imaged sample volume, the sum of all the pixel values in an image is related to the total light intensity scattered from the fuel-air mixture in that plane. Consequently, the input equivalence ratio ϕ can be represented by the average of the pixel values in the image.

The planar scalar concentration data obtained during this study are presented in a number of ways. One representation is contour plots, which depict some measure of the local fuel-air ratio (see Fig. 3). Another example, using false-color pixel intensity maps, is presented in Eaton et al.[22] and a comprehensive collection provided by Frey[18] and Eaton.[19] Yet another approach is to present information as mean equivalence ratio, perhaps as a function of angular position around the premixer circumference. This type of plot clearly illustrates gross mixing features associated with large-scale

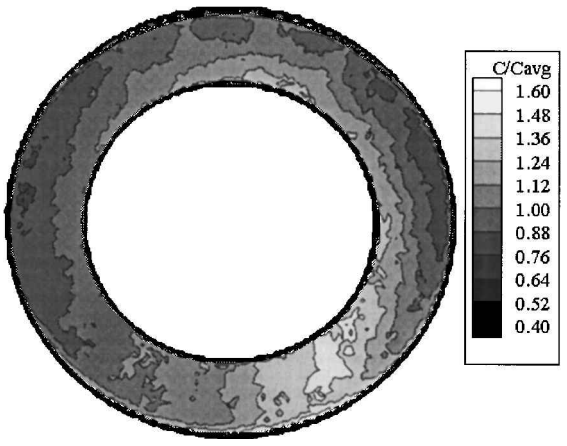

a) Baseline case

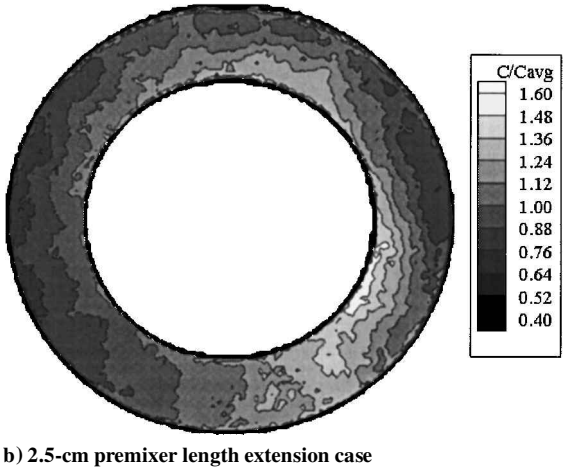

b) 2.5-cm premixer length extension case

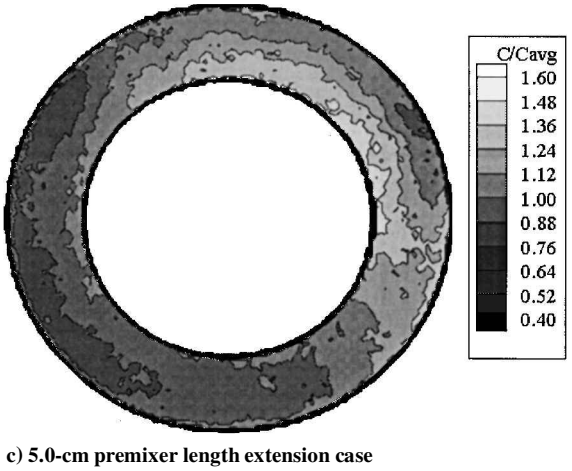

c) 5.0-cm premixer length extension case

Fig. 3 Gray scale images of mixing performance to illustrate the influence of residence time.

motions. Frey[18] and Eaton[19] provide a comprehensive collection of these plots. Selected examples are presented in the Results section.

Another metric provides a local indication of the fluctuation in fuel-air composition. For a given input equivalence ratio a perfectly mixed flow would result in an image with a single pixel value (corresponding to a delta function). One could simply plot the pixel standard deviation values against, say, premixer angular position. However, the standard deviations of two images cannot be compared directly because their overall intensities are likely to be different. Therefore, another quantity was defined to describe mixing in the exit plane of the premixer: the standard deviation divided by the average, also known as the unmixedness parameter s (Ref. 24). The s parameter eliminates the variability between individual averages and allows for direct comparison between data sets. Lower values of this parameter imply better mixing; a perfectly mixed case would have a value of 0%. The majority of the data included in the Results section are presented in terms of s.

Finally, a single figure of merit was computed for each image; the quotient of the standard deviation and mean values for the entire image was formed to yield a global s value. This single number was compared between cases to assess how changes in parameters influenced overall mixing.

III. Results

A. Baseline Case

Mixing information was obtained for the baseline configuration first. A set of 25 corrected images was averaged to form a composite, or average, image. As just mentioned, the figure of merit used to represent the degree of mixing is the ratio of the standard deviation of the pixel intensity values to the average intensity value, or unmixedness parameter. The s value for the baseline composite image is 29%.

To further analyze the characteristics of the baseline case, the composite image was divided into 16 circumferential wedges, or sectors (to correspond with the number of spray bars), and the statistics for each wedge compiled. Figure 4a shows the normalized equivalence ratio around the circumference of the premixer (reported in terms of the normalized average pixel value). Uncertainty bars represent the standard deviation of the means calculated from three separate groups of 25 images each and are shown to illustrate typical repeatability or experimental uncertainty. Obviously, the pixel value (scalar fuel concentration) is not circumferentially uniform around the premixer exit plane. This circumferential variation was associated with the hardware orientation (i.e., when the premixer was rotated, the entire circumferential distribution rotated with it).[19]

Figure 4b shows the circumferential variation of s for the baseline case. The uncertainty bars represent the standard deviation of s for the three baseline runs of 25 images each. This shows the variation in fuel concentration (as denoted by s) within each wedge. The maximum value of s of approximately 24% occurs at $\theta = 80$ deg, whereas the minimum occurs at $\theta = 180$ deg. These values are lower than the s value for the entire image (29%), as expected, because the standard deviation based on a localized area is less than that of a global area for time-averaged results. Also the locations of maxima or minima in the fuel concentration (pixel value in Fig. 4a) do not correspond to extrema in mixing (s), as shown in the dissimilarity in the shapes of the plots in Figs. 4a and 4b. For example, the fuel concentration is relatively constant for $\theta = 0$ to 180 deg, but the mixing level, in contrast, has a sinusoidal trend.

The circumferential variations demonstrate that the fuel was not distributed uniformly by the premixer plenum. Radial variations in fuel concentration were also observed, as discussed by Frey[18] and Eaton.[19] They result from a disproportionate amount of fuel distributed closer to the centerbody. This is easily seen in the contour levels of Fig. 3a, which is a composite image of the entire premixer exit plane. Note the fuel-rich regions around the centerbody compared to the fuel-lean regions at the outer edge of the annulus.

To put our results into perspective, we can compare our data to swirling mixer work from studies that used entirely different experimental techniques. Mello et al.[25] and Barnes and Mellor[26] reported s-parameter values between 10 and 30% at the exit of a similar premixer. They observed that s is a strong function of the mean premixer equivalence ratio. Frazier et al.[27] report s values of 20% near the exit plane of a dual-annular counter rotating swirler-premixer. They also noted that the overall equivalence ratio exhibited maximum spatial variations on the order of 50%.

B. Effects of Inlet Turbulence

Five combinations of turbulence intensity and scale were evaluated to examine the effects of controlled grid inlet turbulence. Two different grids were used to examine the effects of turbulence integral length scale Lx, which is governed by the mesh size of the grid $Lx/D_h = 0.087$ and 0.034, respectively. The intensity of the

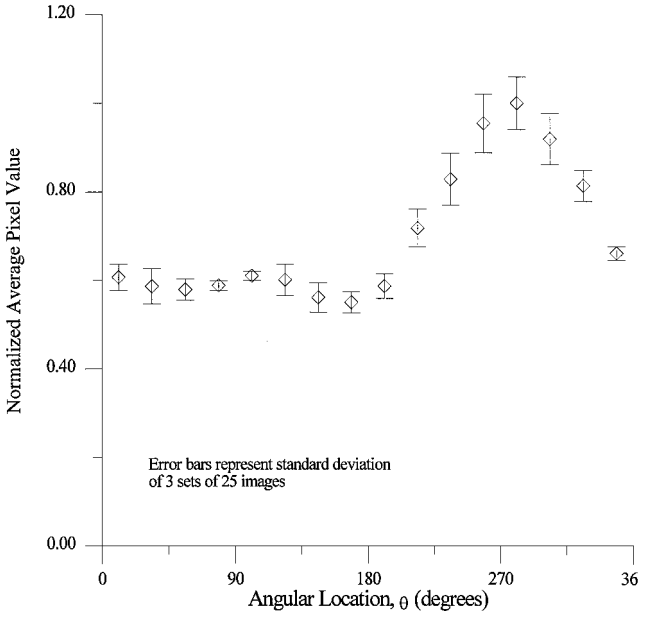

Fig. 4a Baseline normalized average pixel value circumferential variation.

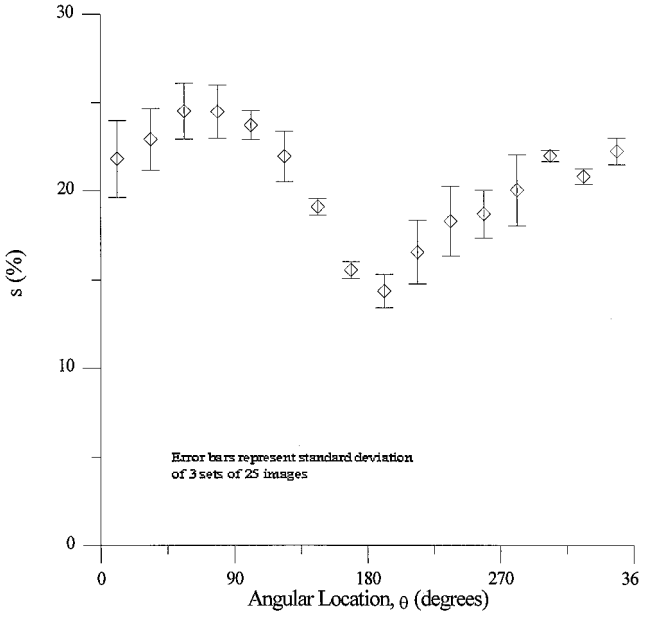

Fig. 4b Baseline unmixedness parameter *s* circumferential variation.

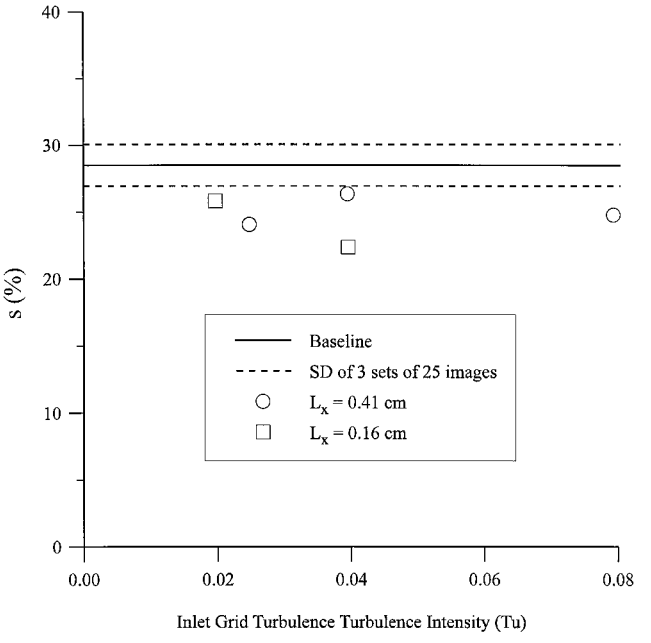

Fig. 5 Unmixedness parameter *s* vs inlet grid turbulence intensity *Tu*.

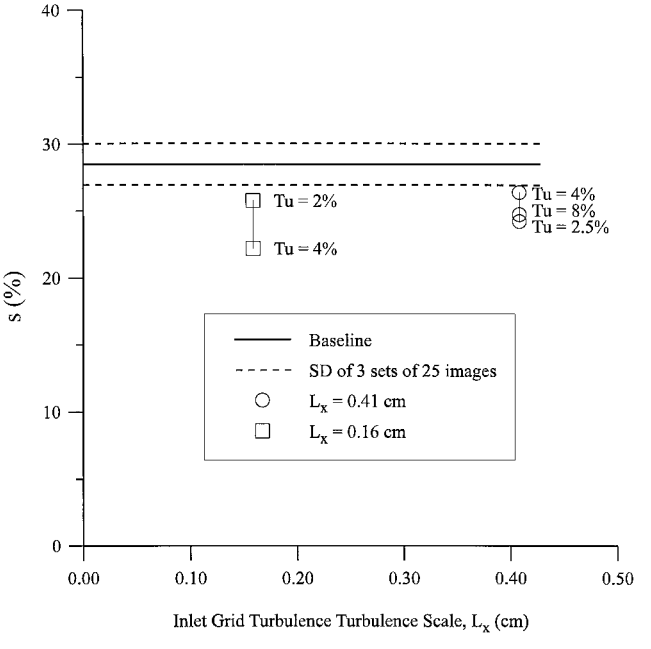

Fig. 6 Unmixedness parameter *s* vs inlet grid turbulence integral length scale *Lx*.

turbulence at the premixer entrance plane was controlled by moving the grid with respect to that plane, thereby allowing the turbulence to decay over a prescribed distance. Turbulence intensities of approximately 2.5, 4, and 8% were generated by the 0.41-cm grid, whereas turbulence intensities of 2 and 4% were generated by the 0.16-cm grid.

The effect of inlet grid turbulence on *s* is shown in Figs. 5 and 6. Figure 5 shows unmixedness *s* vs turbulence intensity *Tu* for the two grids, whereas Fig. 6 illustrates the dependence of *s* on integral length scale for both values of *Lx*. The average for the three baseline (no grid turbulence) runs is shown as a solid line with the dashed line representing the standard deviation of the baseline unmixedness.

Inlet turbulence appears to have improved the mixing only slightly (as indicated by the lower *s* values). For the larger-size 0.41 cm grid the global *s* values for the images of the entire premixer exit plane are 24, 26, and 25% for 2.5, 4, and 8% turbulence intensities, respectively. Similarly, the 0.16 cm grid has global *s* values for the images of the entire exit plane of 26 and 22% for 2 and 4% turbulence intensities. Recall that the corresponding baseline global *s* value for the image of the entire exit plane is 29%. One would generally expect improved mixing with increasing inlet turbulence intensity. However, the $Lx = 0.41$-cm case with $Tu = 2.5\%$ exhibits better mixing than the cases with higher *Tu*. This suggests that both *Lx* and *Tu* are important in affecting the mixing field, which is consistent with the results cited in the Introduction.

Figures 7 and 8 show the circumferential variation of *s* for the elevated inlet turbulence cases. Figure 7 contains data for the 0.41 cm grid. For $\theta = 60$ to 300 deg, the wedge-averaged value of *s* for the 8% turbulence case is less than that for the 4% turbulence case, which is in turn less than that for the 2% turbulence case. This is the expected trend of improved mixing with increasing inlet turbulence intensity. However, there is no obvious trend from $\theta = 0$ to 60 deg or $\theta = 300$ to 360 deg. In these areas the $Tu = 2.5\%$ case curve is lower than for the higher intensity cases, which contributes to the inconsistent behavior of the global *s* value exhibited in Fig. 6.

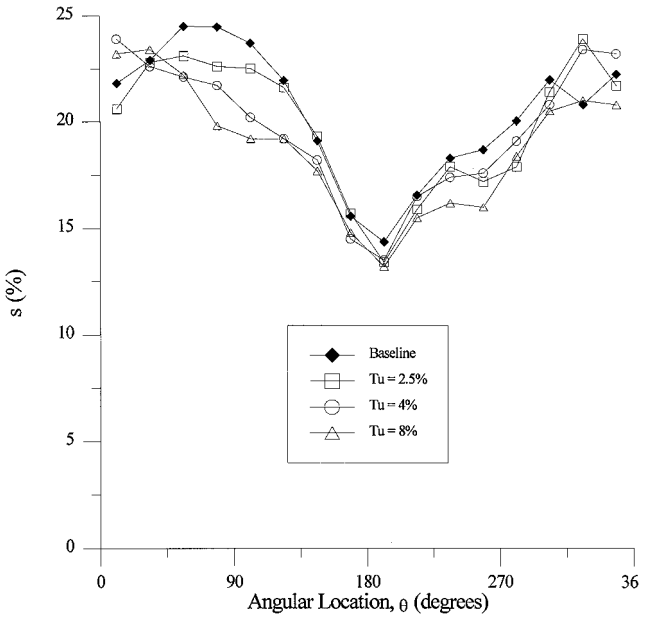

Fig. 7 Circumferential variation in unmixedness parameter *s* for the *M* = 0.41-cm grid.

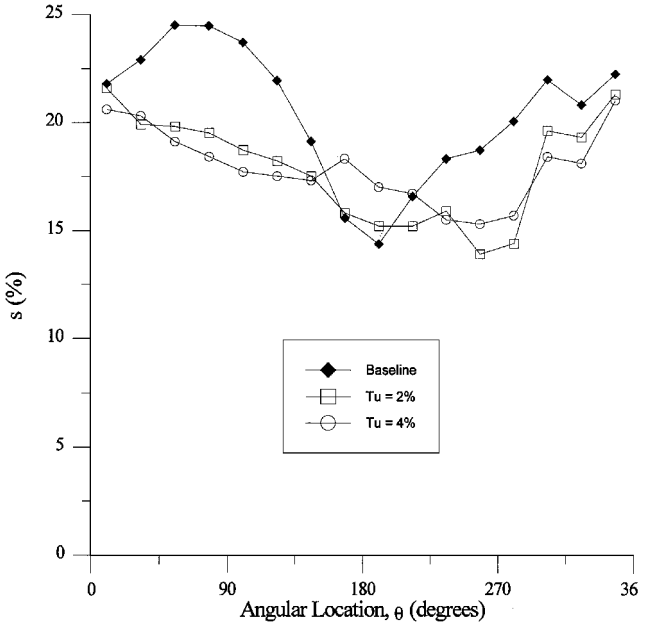

Fig. 8 Circumferential variation in unmixedness parameter *s* for the *M* = 0.16 cm.

Figure 8 is the equivalent graph for the $M = 0.16$-cm grid. The expected trend of improved mixing with increased turbulence intensity occurs for $\theta = 0$ to 145 and 300 to 360 deg, which agrees with the *s* trend for the image as a whole. However, this trend is not apparent from $\theta = 145$ to 300 deg. These results emphasize the complexity of the flowfield and suggest that no single gross metric, such as *Tu*, can be used to characterize mixing in these devices. Detailed studies of the velocity field are necessary to fully understand the wedge-average results.

Radial profile structures for the inlet grid turbulence cases were not significantly different from the baseline case. Interested readers should consult Frey[18] and Eaton.[19]

Although the mixing improved slightly as a result of increasing inlet turbulence, the data are inconclusive (especially the 0.41 cm grid). In light of the high overall turbulence intensity within the premixer generated by the spray bar jets, spray bar wakes, and swirl, this small effect is not surprising. In comparison, the 2.5, 4, and 8% inlet turbulence cases represent incremental turbulence intensity level increases that are insufficient to substantially impact the large-scale mixing. This conclusion is supported by contour plots,[18] where no gross structural changes were apparent when comparing among the various cases.

C. Effects of Premixer Length

Mixing performance for premixer length extensions of 2.5 and 5.0 cm ($L/D_h = 0.53$ and 1.06, respectively) was evaluated to determine the effects of residence time. Figure 9 shows the effect of premixer length on the global value of *s* for the entire image plane. The baseline case is represented by a solid line. The global *s* value for the 2.5-cm premixer length extension is 23%, whereas it is 19% for the 5.0-cm extension case. Comparing both to the baseline case value of 29%, a definite trend of decreasing *s* and, thus, improved mixing with increasing premixer length is found. This is to be expected because adding premixer length increases residence time and should therefore improve mixing. The highly strained swirling flow is conducive to turbulent mixing. However, the magnitude of the effect was not obvious prior to performing the measurements. As a practical matter, it should be mentioned that premixer performance cannot be continually improved simply by increasing premixer length without limit because engine performance will eventually suffer from combustion instability and noise.

To interpret the influence of premixer length extension data, it was important to determine the amount by which the swirling fuel-air mixture rotated from the point at which it was injected until it exited the premixer (i.e., reached the image plane). This was approximated by calculating the solid-body rotation based on the swirl angle of the premixer.

Consider a fuel seed particle that travels an axial distance *x* and a circumferential distance *S* from the point at which it was injected until it exits the premixer. For a given swirl vane angle θ and air velocity V_a, the distances the particle will flow in time *t* can be expressed as follows:

$$x = (V_a \cos\theta)t \tag{2}$$

$$S = (V_a \sin\theta)t \tag{3}$$

Combining equations and solving for *S* yields

$$S = x \tan\theta \tag{4}$$

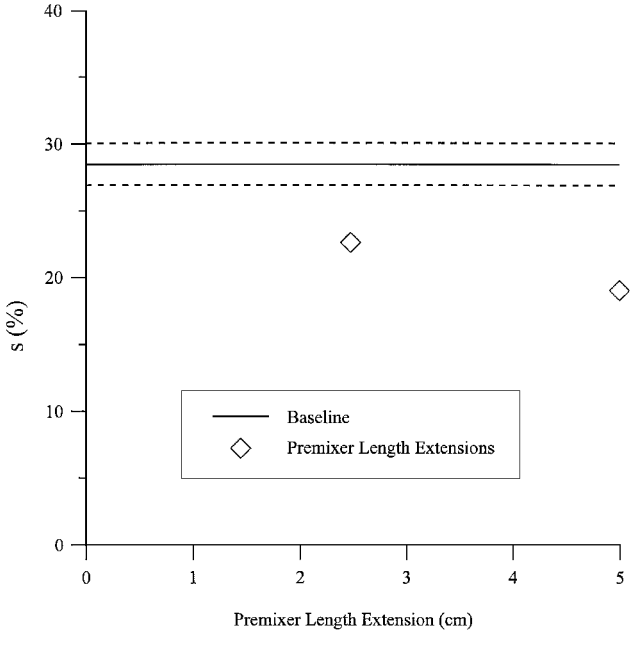

Fig. 9 Unmixedness parameter *s* vs premixer length extension.

Solving for the number of revolutions N

$$N = S/2\pi r = x \tan\theta/2\pi r \quad (5)$$

The inside and outside radii for the premixer are 2.0 and 3.18 cm, respectively. An average value of 2.59 cm was used as an estimate for r. The premixer length is 4.32 cm, and the swirl vane angle is 48 deg. Substituting these values yields $N = 0.29$ revolutions or approximately $\frac{1}{4}$ of a revolution. For each additional premixer length extension of 2.5 cm, an additional 0.17 revolutions is realized.

This value was confirmed experimentally by taping closed a quarter of the fuel spray bars and acquiring an image as in the baseline case configuration. Figure 10a shows the blocked spray bars in the injector plane. Figure 10b is a representation of the resulting gray scale intensity plot at the exit plane. Note that the dark area is approximately $\frac{1}{4}$ of a revolution from the blocked spray bars, which agrees with the solid-body rotation calculation just presented.

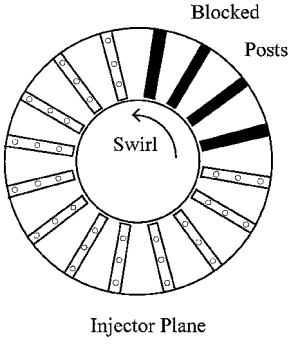

Fig. 10a Fuel spray bars blocked when evaluating solid-body rotation calculations.

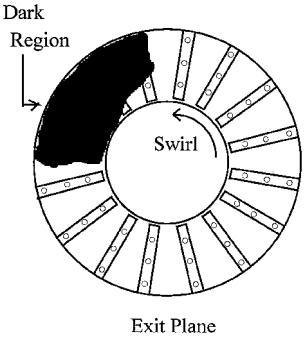

Fig. 10b Representation of gray scale image obtained after blocking fuel spray bars.

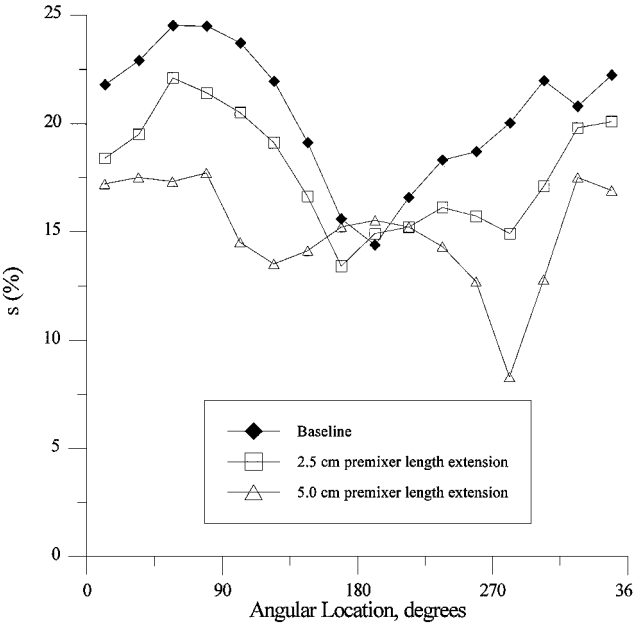

Fig. 11 Premixer length phase-shifted circumferential variation in unmixedness parameter s.

Figure 11 shows phase-shifted circumferential variations in s for the two premixer length extensions and compares them to the baseline case. As expected, mixing was improved with each length addition. Also, variations around the circumference are successively smaller for each increase in length. Compare the gray scale images in Figs. 3a–3c, which correspond to the baseline, 2.5-cm and 5.0-cm extensions, respectively. The circumferential mixing is clearly improved, but the large maldistribution, while mitigated, rotates around the swirler in solid-body rotation.

Radial profiles reported by Frey[18] showed variations for the 5.0-cm premixer length extension to be smaller than those for the 2.5-cm premixer length. This can also be inferred by comparing Figs. 3a–3c. Again, the conclusion is that mixing is improved with premixer length extension both globally and locally.

IV. Conclusions

Large-scale mixing has been evaluated for a swirling gas-turbine premixer. Test conditions included a baseline case, five cases with elevated inlet turbulence, and two premixer length extension cases. Data were presented in terms of the standard deviation in pixel values divided by the mean value, or unmixedness s, in both angularly resolved and global (entire exit plane image) format, as well as contour plots of simulated fuel concentration over the entire exit plane.

The baseline case exhibited fuel concentration nonuniformities, which include a global s value of 29%. Increasing turbulence inlet intensity was found to improve mixing only slightly, with some nonmonotonic results observed when Tu was varied. These nonmonotonic results suggest that at least two properties (e.g., Lx and Tu) are necessary to describe the effects of freestream turbulence on mixing. The effects of relatively low turbulence levels achievable by grids are somewhat masked by locally high turbulence naturally generated in the device, e.g., spray bar wakes. Introducing much higher levels of controlled turbulence (as was done by Ames and coworkers[6,15]) would not be straightforward and may not be practical in applications. For instance, generation of higher levels of turbulence would require a grid of jets—a configuration impractical in a production gas-turbine engine. Finally, there is a definite trend of decreasing global exit plane s and, thus, improved mixing with increasing premixer length. A significant reduction in s, from 29 to 19%, was achieved with a 5.0-cm ($L/D_h = 1.06$) length extension.

These results suggest two conclusions regarding air- and fuel-mixing enhancements. First, implementation of moderate level turbulence generators, such as grids, in premixers is not warranted because the turbulence intensities characteristic of the device are so high that grid-generated turbulence has only a minor effect. Second, increased premixer length is beneficial as it increases residence time and improves mixing.

A complete examination of the velocity field is necessary to complement the scalar field data presented here and to further understand the mixing mechanisms in this complex flow. However, the current results are useful in evaluating choices among competing design concepts.

Acknowledgment

We wish to acknowledge J. P. Gore of Purdue's School of Mechanical Engineering for helpful advice regarding particle seeders.

References

[1] Schorr, M. M., "NO_X Emission Control for Gas Turbines: A 1992 Update on Regulations and Technology," *1992 ASME Cogen-Turbo*, pp. 1–12.

[2] Smith, K. O., and Cowell, L. H., "Experimental Evaluation of a Liquid-Fueled, Lean-Premixed Gas Turbine Combustor," American Society of Mechanical Engineers, Paper 89-GT-264, June 1989.

[3] Smith, K. O., Angello, L. C., and Kurzynske, F. R., "Design and Testing of an Ultra-Low NO_X Gas Turbine Combustor," American Society of Mechanical Engineers, Paper 86-GT-263, June 1986.

[4] Hancock, P. E., and Bradshaw, P., "The Effect of Free-Stream Turbulence on Turbulent Boundary Layer Flow and Heat Transfer," *Journal of Fluids Engineering*, Vol. 105, No. 3, 1983, p. 284.

[5]Blair, M. F., "Influence of Free-Stream Turbulence on Turbulent Boundary Layer Heat Transfer and Mean Profile Development, Part II: Analysis of Results," *Journal of Heat Transfer*, Vol. 105, No. 1, 1983, pp. 41–47.

[6]Ames, F. E., and Moffat, R. J., "Heat Transfer with High Intensity, Large Scale Turbulence: The Flat Plate Turbulent Boundary Layer and the Cylindrical Stagnation Point," Stanford Univ. Rept. HMT-44, Stanford, CA, Oct. 1990.

[7]Goebel, S. G., Abuaf, N., Lovett, J. A., and Lee, C.-P., "Measurements of Combustor Velocity and Turbulence Profiles," American Society of Mechanical Engineers, Paper 93-GT-228, June 1993.

[8]Moss, R. W., and Oldfield, L. G., "Measurements of Hot Combustor Turbulence Spectra," American Society of Mechanical Engineers, Paper 91-GT-351, June 1991.

[9]Moss, R. W., and Oldfield, L. G., "Measurements of the Effect of Free-Stream Turbulence Length Scale on Heat Transfer," American Society of Mechanical Engineers, Paper 92-GT-244, June 1992.

[10]Thole, K. A., and Bogard, D. G., "Enhanced Heat Transfer and Shear Stress Due to High Freestream Turbulence," *Journal of Turbomachinery*, Vol. 117, No. 3, 1995, pp. 418–424.

[11]Bons, J. P., MacArthur, C. D., and Rivir, R. B., "The Effect of High Freestream Turbulence on Film Cooling Effectiveness," American Society of Mechanical Engineers, Paper 94-GT-51, June 1994.

[12]Maciejewski, P. K., and Rivir, R. B., "Effects of Surface Riblets and Free-Stream Turbulence on Heat Transfer in a Linear Turbine Cascade," American Society of Mechanical Engineers, Paper 94-GT-245, June 1994.

[13]Campbell, R. P., and Moffat, R. J., "Discrete Hole Film Cooling on a Convex Wall: Heat Transfer and Hydrodynamics with Free Stream Turbulence," *Heat Transfer in Gas Turbines*, ASME HTD-Vol. 300, edited by M. K. Chyu and N. V. Nirmalan, ASME, New York, 1994, pp. 45–53.

[14]Chen, P.-H., Chen, J.-J., Miao, Z.-M., Chou, S.-F., and Liu, M., "The Effect of Upstream Conditions on the Convective Transport Phenomena over a Turbine Blade," *Heat Transfer in Gas Turbines*, ASME HTD-Vol. 300, edited by M. K. Chyu and N. V. Nirmalan, 1994, pp. 63–81.

[15]Ames, F. E., "The Influence of Large Scale High Intensity Turbulence on Vane Heat Transfer," American Society of Mechanical Engineers, Paper 95-GT-21, June 1995.

[16]Wolochuk, M. C., Plesniak, M. W., and Braun, J. E., "The Effects of Turbulence and Unsteadiness on Vortex Shedding from Sharp-Edged Bluff Bodies," *Journal Fluids Engineering*, Vol. 118, No. 1, 1996, pp. 18–25.

[17]Hinze, J. O., Turbulence, 2nd ed., McGraw–Hill, New York, 1975, pp. 260–275.

[18]Frey, S. F., "Influence of Turbulence Characteristics and Premixer Length on the Performance of an Axial Swirl Premixer," M.S. Thesis, School of Mechanical Engineering, Purdue Univ., West Lafayette, IN, Dec. 1994.

[19]Eaton, A. R., "Influence of Air-to-Fuel Jet Momentum Ratio and Swirling Flow on the Performance of an Axial Swirl Premixer," M.S. Thesis, School of Mechanical Engineering, Purdue Univ., West Lafayette, IN, May 1995.

[20]Bean, H. S. (ed.), *Fluid Meters: Their Theory and Application*, 6th ed., American Society of Mechanical Engineers, New York, 1971, pp. 47–79.

[21]Kounalakis, M. E., "Structure and Radiation Properties of Turbulent Diffusion Flames," Ph.D. Dissertation, Dept. of Aerospace Engineering, Univ. of Michigan, Ann Arbor, MI, 1990.

[22]Eaton, A. R., Frey, S. F., Cusano, D. M., Plesniak, M. W., and Sojka, P. E., "Development of a Full-Field Planar Mie Scattering Technique for Evaluating Swirling Mixers," *Experiments in Fluids*, Vol. 21, No. 5, 1996, pp. 325–330.

[23]Kline, S. J., and McClintock, F. A., "Describing Uncertainties in Single-Sample Experiments," *Mechanical Engineering*, Vol. 75, 1953, pp. 3–9.

[24]Mikus, T., and Heywood, J. B., "The Automotive Gas Turbine and Nitric Oxide Emissions," *Combustion Science and Technology*, Vol. 4, 1971, pp. 149–158.

[25]Mello, J. P., Mellor, A. M., Steele, R. C., and Smith, K. O., "A Study of the Factors Affecting NO_X Emissions in Lean Premixed Turbine Combustors," AIAA Paper 97-2708, July 1997.

[26]Barnes, J. C., and Mellor, A. M., "Quantifying Unmixedness in Lean Premixed Combustors Operating at High Pressure, Fired Conditions," American Society of Mechanical Engineers, Paper 97-GT-73, June 1997.

[27]Frazier, T. R., Foglesong, R. E., Coverdill, R. E., Peters, J. E., and Lucht, R. P., "An Experimental Investigation of Fuel/Air Mixing in an Optically Accessible Axial Premixer," AIAA Paper 98-3543, July 1998.